JACS
JOURNAL OF THE AMERICAN CHEMICAL SOCIETY

Communication

pubs.acs.org/JACS

Signature of Metallic Behavior in the Metal–Organic Frameworks M_3(hexaiminobenzene)$_2$ (M = Ni, Cu)

Jin-Hu Dou,[†] Lei Sun,[†] Yicong Ge,[†] Wenbin Li,[‡] Christopher H. Hendon,[†] Ju Li,[§] Sheraz Gul,[⊥] Junko Yano,[⊥] Eric A. Stach,[#] and Mircea Dincă*[,†]

[†]Department of Chemistry, Massachusetts Institute of Technology, 77 Massachusetts Avenue, Cambridge, Massachusetts 02139, United States

[‡]Research Laboratory of Electronics, Massachusetts Institute of Technology, 77 Massachusetts Avenue, Cambridge, Massachusetts 02139, United States

[§]Department of Nuclear Science and Engineering, Department of Materials Science and Engineering, Massachusetts Institute of Technology, 77 Massachusetts Avenue, Cambridge, Massachusetts 02139, United States

[⊥]Molecular Biophysics and Integrated Bioimaging Division, Lawrence Berkeley National Laboratory, Berkeley, California 94720, United States

[#]Center for Functional Nanomaterials, Brookhaven National Laboratory, Upton, New York 11973, United States

Supporting Information

ABSTRACT: The two-dimensionally connected metal–organic frameworks (MOFs) $Ni_3(HIB)_2$ and $Cu_3(HIB)_2$ (HIB = hexaiminobenzene) are bulk electrical conductors and exhibit ultraviolet-photoelectron spectroscopy (UPS) signatures expected of metallic solids. Electronic band structure calculations confirm that in both materials the Fermi energy lies in a partially filled delocalized band. Together with additional structural characterization and microscopy data, these results represent the first report of metallic behavior and permanent porosity coexisting within a metal–organic framework.

Recent progress in the synthesis of electrically conductive metal–organic frameworks (MOFs) has enabled applications that were previously thought impractical for this traditionally insulating set of materials.[1] Examples include the use of neat MOFs as active electrodes in electrocatalysis,[2,3] batteries,[4,5] chemiresistive sensors,[6,7] thermoelectric devices,[8] supercapacitors,[9] electrochromic devices,[10] and field effect transistors (FETs).[11] Many of these applications are served better by semiconducting MOFs, others would see considerable improvements if the MOFs were metallic. However, there are thus far no examples of metallic MOFs, and demonstrating metallic behavior remains an important challenge of fundamental interest. Along this line, the only materials in this class that exhibit a bulk conductivity greater than 10 S/m at room temperature are Ni_3(2,3,6,7,10,11-hexaiminotriphenylene)$_2$ ($Ni_3(HITP)_2$),[12] Ni_3(benzenehexathiol)$_2$ ($Ni_3(BHT)_2$),[13] and Cu_3(benzenehexathiol)$_2$ ($Cu_3(BHT)_2$).[14] All three belong to a subclass of hexagonal layered structures wherein trigonal organic ligands and square-planar mononuclear metal nodes define two-dimensional (2D) sheets whose electronic structure enables excellent electron delocalization through continuous conjugation.

Relevantly, theoretical studies of these 2D materials predicted that some should behave as bulk metals,[13,15−17] yet experimental evidence for metallic behavior in these remains elusive.[13] We surmised that replacing 2,3,6,7,10,11-hexaiminotriphenylene (HITP) by the smaller hexaiminobenzene (HIB) would reduce the distance and provide better overlap between the electronic wave functions of neighboring metals/ligands in Ni_3(hexaiminobenzene)$_2$ ($Ni_3(HIB)_2$), leading possibly to metallicity. However, recently reported FETs made from films of $M_3(HIB)_2$ (M = Ni, Co, Cu) exhibited responses characteristic of insulators or materials with very low conductance, at best.[18] We contended that this surprisingly insulating behavior was due to the severe disorder and poor crystallinity of the films, as evidenced also by selected area electron diffraction (SAED), and that more crystalline samples would reveal different information about the intrinsic properties of these materials. Accordingly, on the premise that HIB-based frameworks continue to be ideal candidates for metallic MOFs, we set out to devise new synthetic pathways for accessing high quality and crystalline samples of these materials and explore their electrical properties.

Here, we show that crystalline $Ni_3(HIB)_2$ and $Cu_3(HIB)_2$, characterized by X-ray diffraction, spectroscopic analysis, and high resolution transmission electron microscopy (HRTEM), are indeed excellent conductors, with pellet conductivities averaging approximately 1000 S/m at 300 K and under vacuum (Scheme 1). Significantly, ultraviolet-photoelectron spectroscopy (UPS) and electronic band structure calculations evidence intrinsic metallic behavior in both materials.

Black microcrystalline samples of $M_3(HIB)_2$ (M = Ni, Cu) were isolated from reactions of hexaaminobenzene trihydrochloride (HAB·3HCl) with ammoniacal solutions of $Ni(NO_3)_2 \cdot 6H_2O$ or $CuSO_4 \cdot 5H_2O$ in mixtures of water and dimethyl sulfoxide heated at 60 °C in air for 2 h. The presence of O_2 is essential for the isolation of crystalline materials; the absence of air yields only amorphous gray powders. Scanning electron microscopy (SEM) showed that the products consist of

Received: July 11, 2017
Published: September 14, 2017

DOI: 10.1021/jacs.7b07234
J. Am. Chem. Soc. 2017, 139, 13608−13611

Scheme 1. Synthesis of $Ni_3(HIB)_2$ and $Cu_3(HIB)_2$

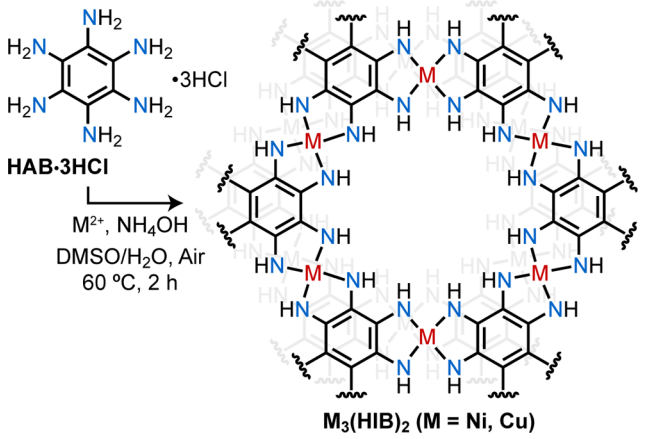

irregularly shaped nanoparticles smaller than 100 nm (Figure S3). Inspection of the M(2p) and N(1s) regions of the high resolution X-ray photoelectron spectra (XPS, Figures S4 and S5) evidenced chemical environments consistent with square planar metal ions and anilinic N atoms in both materials. Additional extra-framework M^{2+} or NH_4^+ ions, the only possible charge-balancing cations for a potentially negatively charged MOF would appear at different regions in the XPS; their absence confirms the neutral state of $M_3(HIB)_2$.

Thermogravimetric analysis (TGA) revealed that both $Ni_3(HIB)_2$ and $Cu_3(HIB)_2$ desolvate above 100 °C and likely decompose above 200 °C, as evidenced by the more pronounced weight losses above this temperature (Figure S6). Evacuation at 120 °C under dynamic vacuum for 24 h followed by N_2 sorption analysis reavealed type II isotherms with uptakes of 82 and 65 cm^3/g at 77 K and apparent Brunauer–Emmett–Teller (BET) surface areas of 152 and 114 m^2/g for $Ni_3(HIB)_2$ and $Cu_3(HIB)_2$, respectively (Figure S7). These values are in line with those of other 2D materials exhibiting similar pore size (vide infra).

Synchrotron powder X-ray diffraction (PXRD) confirmed a high degree of crystallinity: both materials exhibit prominent diffraction peaks at 2θ = 2.54°, 5.18°, 6.81°, 8.10°, 9.07°, 14.27°, and 18.97° (Figures 1, S8, and S9). Indexing of these peaks revealed hexagonal unit cells with lattice parameters a = 13.5(2) Å and c = 3.3(1) Å. To determine the precise interlayer stacking sequence, we performed Ni and Cu K-edge extended X-ray absorption fine structure (EXAFS) analysis. Ni···Ni and Cu···Cu scattering paths at R = 3.60 ± 0.09 Å and R = 3.33 ± 0.10 Å were required to fit the EXAFS spectra of $Ni_3(HIB)_2$ and $Cu_3(HIB)_2$, respectively (Figure S10). Both M···M distances determined by EXAFS analysis exceed the interlayer distance observed by PXRD, suggesting that the 2D layers are not perfectly eclipsed and that significant (ab) shifting occurs in both materials between neighboring layers. Taken together, the PXRD and EXAFS data give structural models where neighboring layers are shifted by approximately one-quarter cell along one edge of the hexagonal unit cell, thereby lowering the symmetry to orthorhombic. Indeed, Le Bail fitting of the PXRD patterns of the two materials gave best fits for space groups $Cmcm$ and $C222_1$ for $Ni_3(HIB)_2$ and $Cu_3(HIB)_2$, respectively (Figure S11), with otherwise identical unit cell parameters a = 13.5(2) Å, b = 23.3(5) Å, and c = 6.6(1) Å.

To understand the difference in symmetry between the Ni and Cu materials, we computed optimized geometries for

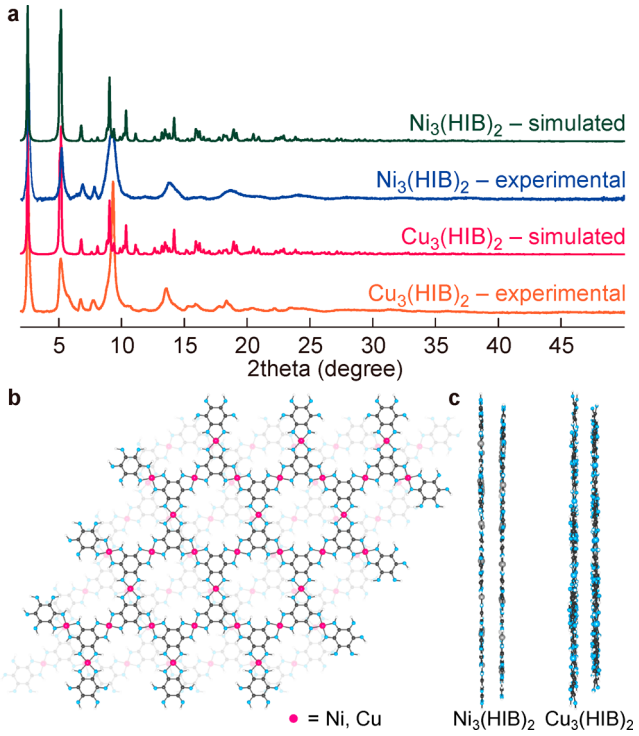

Figure 1. (a) Powder X-ray diffraction patterns. (b,c) Calculated structures of $M_3(HIB)_2$.

individual 2D sheets using density functional theory (DFT) (Figure S12). This revealed hexagonal lattice constants of 13.48 Å, in agreement with the experimental values. It also revealed that the local symmetry of the Ni^{2+} ions is strictly D_{4h}, giving rise to completely planar $Ni_3(HIB)_2$ monolayers, whereas CuN_4 units distort out-of-plane and give rise to overall buckled 2D layers in $Cu_3(HIB)_2$ (Figures 1c and S12). We therefore attribute the lack of mirror symmetry in $Cu_3(HIB)_2$ to the local coordination environment of the Cu^{2+} ions (Figures 1c and S12).

HRTEM provided further evidence of two-dimensional long-range order in $M_3(HIB)_2$. Most notably, fast Fourier transform (FFT) analysis of the images in Figure 2 reavealed honeycomb lattices with a lattice parameter a = 13.5 Å, in excellent agreement with the values obtained from PXRD analysis and DFT computations. Intriguingly, our microscopy and structural data contrasts with that previously reported for these materials.[18] In particular, it suggests a higher degree of

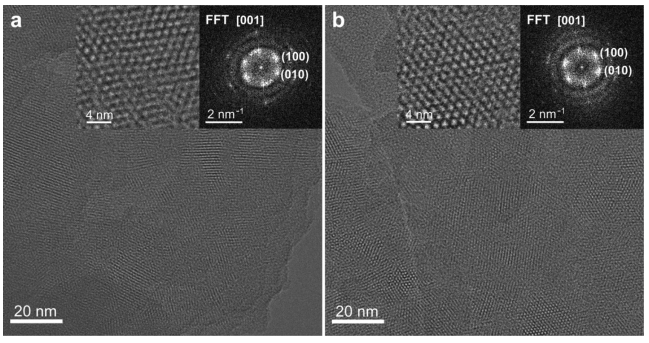

Figure 2. HRTEM image of (a) $Ni_3(HIB)_2$ and (b) $Cu_3(HIB)_2$ taken at 300 kV. Insets are high magnification HRTEM images (left) and the corresponding FFT analysis (right).

DOI: 10.1021/jacs.7b07234
J. Am. Chem. Soc. 2017, 139, 13608–13611

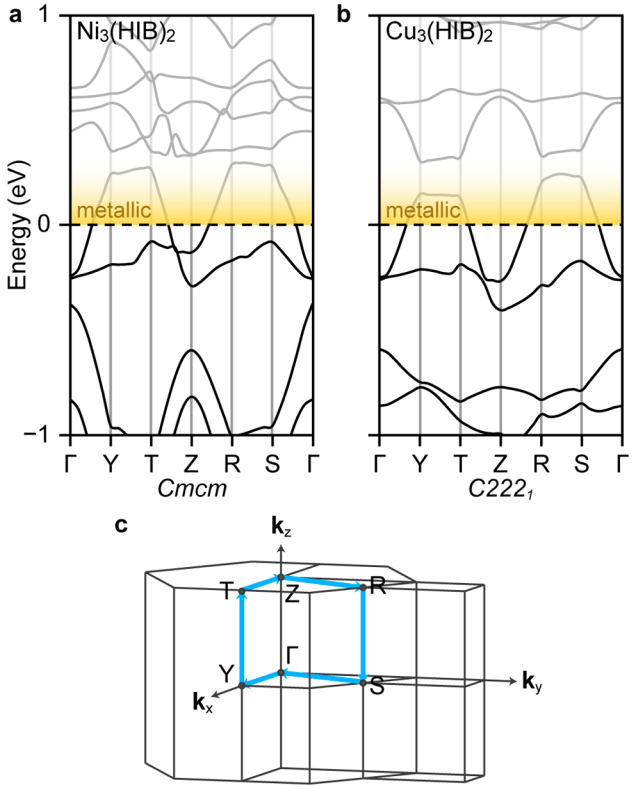

Figure 3. (a,b) Calculated electronic band structure of bulk $Ni_3(HIB)_2$ and $Cu_3(HIB)_2$, respectively. (c) Corresponding first Brillouin zone and high-symmetry K-points.

crystallinity and potentially a different structure for our materials, which encouraged us to investigate the electronic properties of $M_3(HIB)_2$ samples as synthesized here.

Importantly, DFT electronic band structure calculations suggested that both monolayer and bulk $M_3(HIB)_2$ should be metallic. Monolayers of both Ni and Cu MOFs exhibit electronic band structures featuring two wide bands forming a Dirac cone at the K point, reminiscent of the classic Kagome bands (Figure S13).[19] The Dirac bands cross the Fermi level in both Γ−K and Γ−M directions and have wide band dispersions of approximately 0.8 eV. The projected density of states exhibits considerable contributions from the metal, C, and N orbitals at the Fermi level, confirming the high degree of in-plane π-conjugation expected for these materials.

The electronic band structures of bulk orthorhombic $M_3(HIB)_2$ plotted along the high symmetry points in the first Brillouin zone are shown in Figure 3 and Figure S14. Salient features include bands crossing the Fermi level in the in-plane Γ−Y, T−Z, Z−R, and Γ−S directions in both materials, which indicates the metallic character of both solids. Notably, because no bands cross the Fermi level in the out-of-plane directions (Y−T and R−S), the bulk materials are expected to be metallic only in the *ab* directions and semiconducting in the *c* direction.

The bulk electrical properties of $M_3(HIB)_2$ were determined from pelletized samples of the two materials, obtained by pressing powders at approximately 1 GPa. Upon degassing under dynamic vacuum ($\sim 1 \times 10^{-5}$ Torr) at 150 °C, the pellets were imaged with SEM, which revealed small particles with prominent grain boundaries and voids (Figure S15). The electrical conductivity of the pellets, measured by the van der Pauw method (Figure S16) under vacuum and in the dark[20] was 800 S/m for $Ni_3(HIB)_2$ and 1300 S/m in $Cu_3(HIB)_2$ at 300 K.

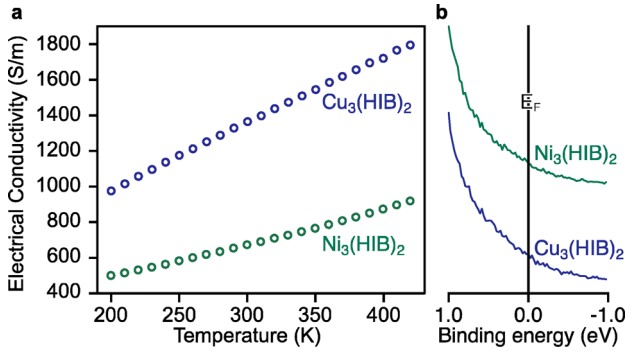

Figure 4. (a) Variable-temperature electrical conductivity of pressed pellets of $M_3(HIB)_2$ measured by the van der Pauw method under vacuum. (b) UPS of $M_3(HIB)_2$ acquired at 300 K.

These are among the highest values observed for MOFs, and compare favorably even with the more relevant subset of electrically conducting 2D MOFs.[1]

Although a signature of bulk metallic behavior is thermally deactivated transport,[21] temperature-dependence conductivity measurements revealed that electrical transport in both $Ni_3(HIB)_2$ and $Cu_3(HIB)_2$ correlates positively with temperature. Indeed, the electrical conductivity in polycrystalline pellets of both MOFs increases linearly as the temperature increases from 200 to 420 K (Figure 4a). PXRD confirmed that no structural transitions occur in this temperature range (Figure S17). We attribute the observed thermally activated transport, more characteristic of semiconducting rather than metallic behavior, to interparticle rather than intraparticle (i.e., intrinsic) transport. In other words, thermally activated hopping over grain boundaries (i.e., interparticle transport) dominates the temperature dependence of conductivity in the bulk polycrystalline pellets, giving rise to apparent semiconducting behavior in otherwise intrinsically metallic solids. This behavior is indeed well documented for granular metals where inter-grain charge hopping mediates charge transport (Figure S18).[22] Further complicating the interpretation of the bulk conductivity of $M_3(HIB)_2$ is the bimodal transport expected from DFT band structure calculations: metallic in the plane of the MOF sheets, but semiconducting normal to the 2D sheets (vide supra). Because the orientation of particles in the pellets is random, both in-plane and out-of-plane charge transport contribute to bulk conductivity, the latter in line with the observed temperature dependence.

Experimental confirmation of the metallic nature of both MOFs came from UPS, which informs on the intrinsic properties of even polycrystalline samples by measuring the density of states near the Fermi level. Grazing incident wide-angle X-ray scattering (GIWAXS) of $Ni_3(HIB)_2$ and $Cu_3(HIB)_2$ films prepared on highly doped silicon (Figure S19), as required for UPS measurements, confirmed the identity of the two MOFs and showed that they preferably orient with a typical face-on packing mode where the 2D sheets are parallel to the silicon substrate (Figure S20).[23] The UPS measurments at 300 K revealed Fermi edges for both $Ni_3(HIB)_2$ and $Cu_3(HIB)_2$ (Figures 4b and S21), which are indicative of electronic bands crossing the Fermi level, and are strong evidence for metallic behavior in $M_3(HIB)_2$.[13,24]

In conclusion, we show that reaction of hexaaminobenzene with Ni^{2+} or Cu^{2+} under carefully controlled conditions gives rise to porous crystalline materials with bulk electrical

DOI: 10.1021/jacs.7b07234
J. Am. Chem. Soc. 2017, 139, 13608−13611

conductivities exceeding 800 S/m. UPS measurements and DFT computational studies evidenced rare metallic behavior in MOFs, a class of notoriously insulating materials. Most importantly, we demonstrate for the first time that metallic behavior and porosity are compatible in these materials. These results encourage further fundamental physical studies and advanced electronic applications, which continue to depend critically on the development of techniques to grow and study single crystals of 2D MOFs, an area of current efforts in our group.

■ ASSOCIATED CONTENT

Supporting Information

The Supporting Information is available free of charge on the ACS Publications website at DOI: 10.1021/jacs.7b07234.

Additional experimental details and characterization data (PDF)

■ AUTHOR INFORMATION

Corresponding Author

*mdinca@mit.edu

ORCID

Jin-Hu Dou: 0000-0002-6920-9051
Lei Sun: 0000-0001-8467-6750
Ju Li: 0000-0002-7841-8058
Junko Yano: 0000-0001-6308-9071
Eric A. Stach: 0000-0002-3366-2153
Mircea Dincă: 0000-0002-1262-1264

Notes

The authors declare no competing financial interest.

■ ACKNOWLEDGMENTS

This work was supported by the Army Research Office (grant number W911NF-17-1-0174). W.L. and J.L. acknowledge support by the Center for Excitonics, an Energy Frontier Research Center funded by U.S. Department of Energy, Office of Science, Basic Energy Sciences under Award No. DE-SC0001088. We thank Dr. Xiaolong Li at beamline BL14B1 (Shanghai Synchrotron Radiation Facility) for assistance with the GIWAXS experiments. Aberration-corrected TEM was carried out at the Center for Functional Nanomaterials, Brookhaven National Laboratory, which is supported by the U.S. Department of Energy. Use of the Advanced Photon Source at Argonne National Laboratory was supported by the U.S. Department of Energy, Office of Science, Office of Basic Energy Sciences, under Contract No. DE-AC02-06CH11357. Part of this work (XAS data collection) was carried out at Stanford Synchrotron Radiation Lightsource, SLAC National Accelerator Laboratory, supported by the U.S. Department of Energy, Office of Science, Office of Basic Energy Sciences under Contract No. DE-AC02-76SF00515. XAS studies were performed with support of the Office of Science, OBES, Division of Chemical Sciences, Geosciences, and Biosciences (CSGB) of the DOE under contract no. DE-AC02-05CH11231 (J.Y.). We thank Dr. Charles Settens for assistance with in situ X-ray diffraction measurements. Part of the characterization and device fabrication was performed at the Harvard Center for Nanoscale Systems (CNS), a member of the National Nanotechnology Infrastructure Network (NNIN), which is supported by the National Science Foundation under NSF award no. ECS-0335765 This work used the Extreme Science and Engineering Discovery Environment (XSEDE), which is supported by the National Science Foundation grant number ACI-1053575.

■ REFERENCES

(1) Sun, L.; Campbell, M. G.; Dincă, M. *Angew. Chem., Int. Ed.* **2016**, *55*, 3566−3579.
(2) Miner, E. M.; Fukushima, T.; Sheberla, D.; Sun, L.; Surendranath, Y.; Dincă, M. *Nat. Commun.* **2016**, *7*, 10942.
(3) (a) Clough, A. J.; Yoo, J. W.; Mecklenburg, M. H.; Marinescu, S. C. *J. Am. Chem. Soc.* **2015**, *137*, 118−121. (b) Zhao, S.; Wang, Y.; Dong, J.; He, C.-T.; Yin, H.; An, P.; Zhao, K.; Zhang, X.; Gao, C.; Zhang, L.; Lv, J.; Wang, J.; Zhang, J.; Khattak, A. M.; Khan, N. A.; Wei, Z.; Zhang, J.; Liu, S.; Zhao, H.; Tang, Z. *Nat. Energy* **2016**, *1*, 16184.
(4) Aubrey, M. L.; Long, J. R. *J. Am. Chem. Soc.* **2015**, *137*, 13594−13602.
(5) Zhang, Z.; Yoshikawa, H.; Awaga, K. *J. Am. Chem. Soc.* **2014**, *136*, 16112−16115.
(6) Campbell, M. G.; Sheberla, D.; Liu, S. F.; Swager, T. M.; Dincă, M. *Angew. Chem., Int. Ed.* **2015**, *54*, 4349−4352.
(7) Campbell, M. G.; Liu, S. F.; Swager, T. M.; Dincă, M. *J. Am. Chem. Soc.* **2015**, *137*, 13780−13783.
(8) Erickson, K. J.; Leonard, F.; Stavila, V.; Foster, M. E.; Spataru, C. D.; Jones, R. E.; Foley, B. M.; Hopkins, P. E.; Allendorf, M. D.; Talin, A. A. *Adv. Mater.* **2015**, *27*, 3453−3459.
(9) Sheberla, D.; Bachman, J. C.; Elias, J. S.; Sun, C.; Shao-Horn, Y.; Dincă, M. *Nat. Mater.* **2017**, *16*, 220−224.
(10) AlKaabi, K.; Wade, C. R.; Dincă, M. *Chem.* **2016**, *1*, 264−272.
(11) Wu, G.; Huang, J.; Zang, Y.; He, J.; Xu, G. *J. Am. Chem. Soc.* **2017**, *139*, 1360−1363.
(12) Sheberla, D.; Sun, L.; Blood-Forsythe, M. A.; Er, S.; Wade, C. R.; Brozek, C. K.; Aspuru-Guzik, A.; Dincă, M. *J. Am. Chem. Soc.* **2014**, *136*, 8859−8862.
(13) Kambe, T.; Sakamoto, R.; Kusamoto, T.; Pal, T.; Fukui, N.; Hoshiko, K.; Shimojima, T.; Wang, Z.; Hirahara, T.; Ishizaka, K.; Hasegawa, S.; Liu, F.; Nishihara, H. *J. Am. Chem. Soc.* **2014**, *136*, 14357−14360.
(14) Huang, X.; Sheng, P.; Tu, Z.; Zhang, F.; Wang, J.; Geng, H.; Zou, Y.; Di, C.-A.; Yi, Y.; Sun, Y.; Xu, W.; Zhu, D. *Nat. Commun.* **2015**, *6*, 7408.
(15) Chen, S.; Dai, J.; Zeng, X. C. *Phys. Chem. Chem. Phys.* **2015**, *17*, 5954−5958.
(16) Yamada, M. G.; Soejima, T.; Tsuji, N.; Hirai, D.; Dincă, M.; Aoki, H. *Phys. Rev. B: Condens. Matter Mater. Phys.* **2016**, *94*, 081102.
(17) Wu, M.; Wang, Z.; Liu, J.; Li, W.; Fu, H.; Sun, L.; Liu, X.; Pan, M.; Weng, H.; Dincă, M.; Fu, L.; Li, J. *2D Mater.* **2017**, *4*, 015015.
(18) Lahiri, N.; Lotfizadeh, N.; Tsuchikawa, R.; Deshpande, V. V.; Louie, J. *J. Am. Chem. Soc.* **2017**, *139*, 19−22.
(19) Chisnell, R.; Helton, J. S.; Freedman, D. E.; Singh, D. K.; Bewley, R. I.; Nocera, D. G.; Lee, Y. S. *Phys. Rev. Lett.* **2015**, *115*, 147201.
(20) Sun, L.; Park, S. S.; Sheberla, D.; Dincă, M. *J. Am. Chem. Soc.* **2016**, *138*, 14772−14782.
(21) Kobayashi, H.; Cui, H.; Kobayashi, A. *Chem. Rev.* **2004**, *104*, 5265−5288.
(22) Beloborodov, I. S.; Lopatin, A. V.; Vinokur, V. M.; Efetov, K. B. *Rev. Mod. Phys.* **2007**, *79*, 469−518.
(23) Cho, E.; Risko, C.; Kim, D.; Gysel, R.; Miller, N. C.; Breiby, D. W.; McGehee, M. D.; Toney, M. F.; Kline, R. J.; Brédas, J.-L. *J. Am. Chem. Soc.* **2012**, *134*, 6177−6190.
(24) Stassen, I.; Burtch, N.; Talin, A.; Falcaro, P.; Allendorf, M.; Ameloot, R. *Chem. Soc. Rev.* **2017**, *46*, 3185−3241.

■ NOTE ADDED IN PROOF

A publication on a similar topic appeared while this manuscript was under review. See: Clough, A. J.; Skelton, J. M.; Downes, C. A.; De la Rosa, A.; Yoo, J. W.; Walsh, A.; Melot, B. C.; Marinescu, S.C. *J. Am. Chem. Soc.* **2017**, *139*, 10863−10867.

DOI: 10.1021/jacs.7b07234
J. Am. Chem. Soc. 2017, 139, 13608−13611